Research Article | Vol. 26, No. 12 | 11 Jun 2018 | OPTICS EXPRESS 14915
Optics EXPRESS

X-ray ptychography using randomized zone plates

G. R. Morrison,[1,2,*] F. Zhang,[1,2,3] A. Gianoncelli,[4] and I. K. Robinson[1,2,5]

[1] *University College London, London Centre for Nanotechnology, 17-19 Gordon St., London WC1H 0AH, UK*
[2] *Research Complex at Harwell, Rutherford Appleton Laboratory, Didcot OX11 0FA, UK*
[3] *Department of Electrical and Electronic Engineering, Southern University of Science and Technology, Shenzhen 518055, China*
[4] *Elettra – Sincrotrone Trieste S.C.p.A., S.S. 14, km 163.5 in Area Science Park, 34149 Trieste, Italy*
[5] *Condensed Matter Physics and Materials Department, Brookhaven National Lab, Upton, New York 11973, USA*
[*] *graeme.morrison@ucl.ac.uk*

Abstract: We have developed a randomized grating condenser zone plate (GCZP) that provides a μm-scale probe for use in x-ray ptychography. This delivers a significantly better x-ray throughput than probes defined by pinhole apertures, while providing a clearly-defined level of phase diversity to the illumination on the sample, and helping to reduce the dynamic range of the detected signal by spreading the zero-order light over an extended area of the detector. The first use of this novel x-ray optical element has been demonstrated successfully for both amplitude and phase contrast imaging using soft x-rays on the TwinMic beamline at the Elettra synchrotron.

OCIS codes: (340.0340) X-ray optics; (050.1970) Diffractive optics; (110.1650) Coherence imaging; (340.7460) X-ray microscopy.

References and links

1. H. N. Chapman and K. A. Nugent, "Coherent lensless X-ray imaging," Nat. Photon. **4**, 833–839 (2010).
2. K. A. Nugent, "Coherent methods in the X-ray sciences," Adv. Phys. **59**, 1–99 (2010).
3. J. M. Rodenburg, A. C. Hurst, A. G. Cullis, B. R. Dobson, F. Pfeiffer, O. Bunk, C. David, K. Jefimovs, and I. Johnson, "Hard-x-ray lensless imaging of extended objects," Phys. Rev. Lett. **98**, 034801 (2007).
4. P. Thibault, M. Dierolf, A. Menzel, O. Bunk, C. David, and F. Pfeiffer, "High-resolution scanning x-ray diffraction microscopy," Science. **321**, 379–382 (2008).
5. A. M. Maiden and J. M. Rodenburg, "An improved ptychographical phase retrieval algorithm for diffractive imaging," Ultramicroscopy. **109**, 1256–1262 (2009).
6. P. Thibault and M. Guizar-Sicairos, "Maximum-likelihood refinement for coherent diffractive imaging," New J. Phys. **14**, 063004 (2012).
7. S. Marchesini, A. Schirotzek, C. Yang, H.-T. Wu, and F. Maia, "Augmented projections for ptychographic imaging," Inverse Probl. **29**, 115009 (2013).
8. A. M. Maiden, M. J. Humphry, M. C. Sarahan, B. Kraus, and J. M. Rodenburg, "An annealing algorithm to correct positioning errors in ptychography," Ultramicroscopy. **120**, 64–72 (2012).
9. F. Zhang, I. Peterson, J. Vila-Comamala, A. Diaz, F. Berenguer, R. Bean, B. Chen, A. Menzel, I. K. Robinson, and J. M. Rodenburg, "Translation position determination in ptychographic coherent diffraction imaging," Opt. Express **21**, 13592–13606 (2013).
10. M. Guizar-Sicairos, M. Holler, A. Diaz, J. Vila-Comamala, O. Bunk, and A. Menzel, "Role of the illumination spatial-frequency spectrum for ptychography," Phys. Rev. B **86**, 100103 (2012).
11. N. Burdet, G. R. Morrison, X. Huang, X. Shi, J. N. Clark, F. Zhang, M. Civita, R. Harder, and I. K. Robinson, "Observations of artefacts in the x-ray ptychography method," Opt. Express **22**, 10294–10303 (2014).
12. A. Fannjiang and W. Liao, "Phase retrieval with random phase illumination," J. Opt. Soc. Am. A **29**, 1847–1859 (2012).
13. A. Fannjiang and W. Liao, "Fourier phasing with phase-uncertain mask," Inverse Probl. **29**, 125001 (2013).
14. J. C. da Silva and A. Menzel, "Elementary signals in ptychography," Opt. Express **23**, 33812–33821 (2015).

#325987 https://doi.org/10.1364/OE.26.014915
Journal © 2018 Received 13 Mar 2018; revised 26 Apr 2018; accepted 6 May 2018; published 29 May 2018

Optics EXPRESS

15. P. Chen and A. Fannjiang, "Coded aperture ptychography: uniqueness and reconstruction," Inverse Prob. **34**, 025003 (2018).
16. O. Bunk, M. Dierolf, S. Kynde, I. Johnson, O. Marti, and F. Pfeiffer, "Influence of the overlap parameter on the convergence of the ptychographical iterative engine," Ultramicroscopy. **108**, 481–487 (2008).
17. T. B. Edo, D. J. Batey, A. M. Maiden, C. Rau, U. Wagner, Z. D. Pešić, T. A. Waigh, and J. M. Rodenburg, "Sampling in x-ray ptychography," Phys. Rev. A **87**, 053850 (2013).
18. D. J. Batey, T. B. Edo, C. Rau, U. Wagner, Z. D. Pešić, T. A. Waigh, and J. M. Rodenburg, "Reciprocal-space up-sampling from real-space oversampling in x-ray ptychography," Phys. Rev. A **89**, 043812 (2014).
19. Y.-S. Shi, Y.-L. Wang, and S.-G. Zhang, "Generalized Ptychography with Diverse Probes," Chin. Phys. Lett. **30**, 054203 (2013).
20. S. M. Gruner, M. W. Tate, and E. F. Eikenberry, "Charge-coupled device area x-ray detectors," Rev. Sci. Instrum. **73**, 2815–2842 (2002).
21. A. Gianoncelli, G. R. Morrison, B. Kaulich, D. Bacescu, and J. Kovac, "Scanning transmission x-ray microscopy with a configurable detector," Appl. Phys. Lett. **89**, 251117 (2006).
22. H. Liu, Z. Xu, X. Zhang, Y. Wu, Z. Guo, and R. Tai, "Effects of missing low-frequency information on ptychographic and plane-wave coherent diffraction imaging," Appl. Opt. **52**, 2416–2427 (2013).
23. R. N. Wilke, M. Vassholz, and T. Salditt, "Semi-transparent central stop in high-resolution X-ray ptychography using Kirkpatrick–Baez focusing," Acta Crystallogr. Sect. A **69**, 490–497 (2013).
24. A. Suzuki, K. Shimomura, M. Hirose, N. Burdet, and Y. Takahashi, "Dark-field X-ray ptychography: Towards high-resolution imaging of thick and unstained biological specimens," Sci. Rep. **6**, 35060 (2016).
25. M. Rose, T. Senkbeil, A. R. von Gundlach, S. Stuhr, C. Rumancev, D. Dzhigaev, I. Besedin, P. Skopintsev, L. Loetgering, J. Viefhaus, A. Rosenhahn, and I. A. Vartanyants, "Quantitative ptychographic bio-imaging in the water window," Opt. Express **26**, 1237–1254 (2018).
26. D. A. Shapiro, Y.-S. Yu, T. Tyliszczak, J. Cabana, R. Celestre, W. Chao, K. Kaznatcheev, K. L. David, F. Maia, S. Marchesini, Y. S. Meng, T. Warwick, L. L. Yang, and H. A. Padmore, "Chemical composition mapping with nanometre resolution by soft X-ray microscopy," Nat. Photon. **8**, 765–769 (2014).
27. K. Giewekemeyer, M. Beckers, T. Gorniak, M. Grunze, T. Salditt, and A. Rosenhahn, "Ptychographic coherent x-ray diffractive imaging in the water window," Opt. Express **19**, 1037–1050 (2011).
28. F. Zhang, G. Pedrini, and W. Osten, "Phase retrieval of arbitrary complex-valued fields through aperture-plane modulation," Phys. Rev. A **75**, 043805 (2007).
29. A. M. Maiden, J. M. Rodenburg, and M. J. Humphry, "Optical ptychography: a practical implementation with useful resolution," Opt. Lett. **35**, 2585–2587 (2010).
30. A. M. Maiden, G. R. Morrison, B. Kaulich, A. Gianoncelli, and J. M. Rodenburg, "Soft X-ray spectromicroscopy using ptychography with randomly phased illumination," Nat. Commun. **4**, 1669 (2013).
31. F. Zhang, B. Chen, G. R. Morrison, J. Vila Comamala, M. Guizar-Sicairos, and I. K. Robinson, "Phase Retrieval by Coherent Modulation Imaging," Nat. Commun. **7**, 13367 (2016).
32. U. Vogt, M. Lindblom, P. Charalambous, B. Kaulich, and T. Wilhein, "Condenser for Koehler-like illumination in transmission x-ray microscopes at undulator sources," Opt. Lett. **31**, 1465–1467 (2006).
33. A. Takeuchi, K. Uesugi, and Y. Suzuki, "Zernike phase-contrast x-ray microscope with pseudo-Kohler illumination generated by sectored (polygon) condenser plate," J. Phys.: Conf. Ser. **186**, 012020 (2009).
34. D. J. Stigliani Jr, R. Mittra, and R. G. Semonin, "Resolving Power of a Zone Plate," J. Opt. Soc. Am. **57**, 610–613 (1967).
35. B. Kaulich, D. Bacescu, J. Susini, C. David, E. di Fabrizio, G. R. Morrison, P. S. Charalambous, J. Thieme, T. Wilhein, J. Kovac, D. Cocco, M. Salomé, O. Dhez, T. Weitkamp, S. Cabrini, D. Cojoc, A. Gianoncelli, U. Vogt, M. Podnar, M. Zangrando, M. Zacchigna, and M. Kiskinova, "TwinMic – a European twin x-ray microscopy station commissioned at ELETTRA," in "Proc. 8th Int. Conf. X-ray Microscopy," S. Aoki, Y. Kagoshima, and Y. Suzuki, eds., vol. 7 of *IPAP Conf. Ser.* (IPAP, Tokyo, 2006), pp. 22–25.
36. A. Gianoncelli, G. Kourousias, L. Merolle, M. Altissimo, and A. Bianco, "Current status of the TwinMic beamline at Elettra: a soft X-ray transmission and emission microscopy station," J. Synchrotron Radiat. **23**, 1526–1527 (2016).
37. M. Dierolf, P. Thibault, A. Menzel, C. M. Kewish, K. Jefimovs, I. Schlichting, K. Von Koenig, O. Bunk, and F. Pfeiffer, "Ptychographic coherent diffractive imaging of weakly scattering specimens," New J. Phys. **12**, 035017 (2010).
38. X. Huang, H. Yan, R. Harder, Y. Hwu, I. K. Robinson, and Y. S. Chu, "Optimization of overlap uniformness for ptychography," Opt. Express **22**, 12634–12644 (2014).
39. P. S. Charalambous, ZonePlates Ltd, London, UK, `www.zoneplates.com`. Accessed 25-Apr-2018.
40. F. Zhang, I. Yamaguchi, and L. P. Yaroslavsky, "Algorithm for reconstruction of digital holograms with adjustable magnification," Opt. Lett. **29**, 1668–1670 (2004).
41. B. Henke, E. Gullikson, and J. Davis, "X-ray interactions: photoabsorption, scattering, transmission, and reflection at E=50-30000 eV, Z=1-92," Atom. Data Nucl. Data **54**, 181–342 (1993).
42. P. S. Charalambous, ZonePlates Ltd, London, UK, (personal communication, 2018).
43. M. W. Jones, B. Abbey, A. Gianoncelli, E. Balaur, C. Millet, M. B. Luu, H. D. Coughlan, A. J. Carroll, A. G. Peele, L. Tilley, and G. A. van Riessen, "Phase-diverse Fresnel coherent diffractive imaging of malaria parasite-infected red blood cells in the water window," Opt. Express **21**, 32151–32159 (2013).
44. C. Jacobsen, J. Deng, and Y. Nashed, "Strategies for high-throughput focused-beam ptychography," J. Synchrotron

Optics EXPRESS

Radiat. **24**, 1078–1081 (2017).
45. L. Kipp, M. Skibowski, R. L. Johnson, R. Berndt, R. Adelung, S. Harm, and R. Seemann, "Sharper images by focusing soft X-rays with photon sieves," Nature. **414**, 184–188 (2001).
46. E. Di Fabrizio, D. Cojoc, S. Cabrini, B. Kaulich, J. Susini, P. Facci, and T. Wilhein, "Diffractive optical elements for differential interference contrast x-ray microscopy," Opt. Express **11**, 2278–2288 (2003).
47. E. Di Fabrizio, D. Cojoc, S. Cabrini, M. Altissimo, B. Kaulich, T. Wilhein, J. Susini, and O. Dhez, "Phase and intensity control through diffractive optical elements in X-ray microscopy," J. Electron Spectrosc. Relat. Phenom. **144–147**, 957–961 (2005).
48. D. Cojoc, B. Kaulich, A. Carpentiero, S. Cabrini, L. Businaro, and E. Di Fabrizio, "X-ray vortices with high topological charge," Microelectron. Eng. **83**, 1360–1363 (2006).
49. S. Marchesini, Y.-C. Tu, and H.-T. Wu, "Alternating projection, ptychographic imaging and phase synchronization," Appl. Comput. Harmon. Anal. **41**, 815–851 (2016).
50. D. R. Luke, "Relaxed averaged alternating reflections for diffraction imaging," Inverse Prob. **21**, 37–50 (2005).

1. Introduction

In recent years coherent diffraction imaging (CDI) techniques have exploited the very high brightness available at the latest generation of x-ray sources to provide high resolution imaging capabilities that can recover the full complex wavefield on the exit surface of the sample [1, 2]. A particularly successful approach has been x-ray ptychography [3], which can be considered a hybrid of CDI and scanning transmission x-ray microscopy (STXM) that allows the imaging of extended objects with a spatial resolution that is significantly better than the lateral dimensions of the x-ray probe. This is particularly attractive for x-ray imaging, where it is technically challenging and very expensive to produce high quality focusing optics that are capable of providing lateral resolutions of better than a few tens of nanometers. Diffraction patterns are recorded from overlapping areas of the sample, and iterative algorithms allow simultaneous retrieval of amplitude and phase information about both the illuminating probe and the wavefront on the exit surface of the sample [4–7]. The redundancy in the data fed into these algorithms enhances the speed and stability of their convergence towards consistent reconstructions of the complex amplitudes, and this has led to algorithm variants that can also determine accurately the probe positions on the sample [8, 9]. Increasing the diversity of the illuminating probe's amplitude or phase has been found to improve the quality of image reconstructions in diffractive imaging, both from empirical observations [10, 11] and from a theoretical perspective [12–15].

In ptychography it is essential that there is significant overlap between adjacent illuminated regions of the sample. This is typically $\sim 60\%$ of the probe linear dimensions [16], but other sampling strategies can also be used [14, 17, 18]. A large number of probe positions may be needed when scanning with a small probe, so it can be helpful to use a relatively large probe, to enable extended sample areas to be surveyed with a modest number of probe positions. Ptychography can be used successfully with a variety of different probe shapes [19], and the probe can be defined by an aperture, or by a focusing element. In the case of an aperture the zero-order signal on the detector, arising from light that has not been diffracted by the aperture, scales with the square of the aperture area, so large apertures significantly increase the dynamic range of the detected signal, which is not well matched to the capabilities of many 2D x-ray detectors, particularly at soft x-ray wavelengths where charge-coupled devices (CCDs) are commonly used [20, 21]. The difficulties caused by a relatively large dynamic range can be tackled in a number of ways: by using an axial beam stop or attenuator to reduce the zero-order signal [22–25], by merging the data acquired using short and long exposure times [3, 26], or by accumulating the signal from many short exposures [27]. Introducing a diffuser into the beam path to enhance the phase diversity has the beneficial effect of spreading the diffracted signal over a larger area of the detector, thereby reducing its dynamic range [28–31]. The use of a focused probe can also reduce the dynamic range of the signal landing on a far-field detector, as the diverging beam downstream of the focal plane spreads the zero-order signal over an extended area of the detector. Simply defocusing a small probe is therefore one way to form a larger spot from an existing high-resolution focusing

Optics EXPRESS

element, although then the shape of the probe will clearly vary with the chosen defocus. In this paper we describe the first use of a novel form of phase-randomized grating condenser zone plate (GCZP) that can produce micron-scale x-ray probes with an enhanced and well-defined phase diversity, and much higher signal throughput than the combination of a probe-defining aperture and an x-ray diffuser that has previously been used in x-ray ptychography [30].

2. Experimental setup

GCZPs for x-rays were developed [32, 33] to produce locally homogeneous illumination of the sample plane in a transmission x-ray microscope (TXM). As shown in Fig. 1, a GCZP is an approximation to a conventional Fresnel zone plate (FZP). An FZP consists of concentric annular zones with a decreasing radial spacing between successive zone boundaries. A GCZP, with inner and outer radii that are the same as for the FZP, is generated by replacing the annular zones with concentric polygonal shells whose sides form the inner edges of a set of linear gratings, as shown in Fig. 1(b). Within each shell the grating periods are chosen so that the positive first-order diffracted beams are all directed to overlap one another on the optical axis at the same focal distance as the FZP in Fig. 1(a). For a GCZP of the type shown in Fig. 1(b), the individual gratings are all square and the same size, so that they make equal contributions to the total signal in the focal spot. When illuminated by a coherent plane wave a conventional FZP produces a focal spot that is similar to an Airy ring pattern [34], with a width proportional to the outermost zone width, whereas the GCZP generates a focal spot whose diameter is determined by the size of the individual gratings. The linear gratings do not focus the beams, but diffraction from the square aperture of the gratings does broaden the beams before they overlap in the focal plane.

The GCZP shown in Fig. 1(c) is a modified form of that in Fig. 1(b), in which the individual grating positions have all been randomized. The angular start position of each shell of gratings has a random offset added to it and each grating has a random radial offset up to a maximum of one period of that grating. The net effect is that the randomized GCZP produces a focal spot similar to that of the regular GCZP, except that there is a random phase term associated with each of the diffracted beams contributing to the focal spot. The randomized GCZP thus provides a means of generating a focused x-ray probe with a well-defined level of phase diversity, set by the number of gratings in the GCZP pattern.

The TwinMic end-station at Elettra has both STXM and TXM modes of operation [35, 36]. For ptychography measurements, the STXM system controls the alignment of all the optical elements upstream of the sample, and the scanning of the sample stage through the x-ray beam. For the results reported here the scan path took the form of an Archimedes spiral where the

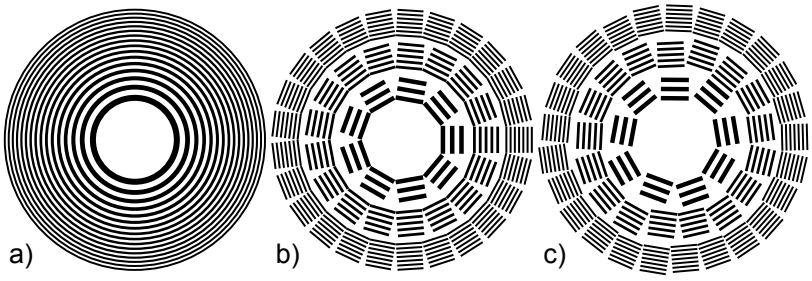

Fig. 1. Schematic diagrams showing a) a conventional Fresnel zone plate with the two innermost zones blanked, b) a grating condenser zone plate with inner and outer radii that are the same as for the Fresnel zone plate in (a), and c) a similar grating condenser zone plate to that shown in (b), but with randomized grating positions. In all three parts of the figure, black denotes areas that are transparent, and white shows areas that are opaque.

Optics EXPRESS

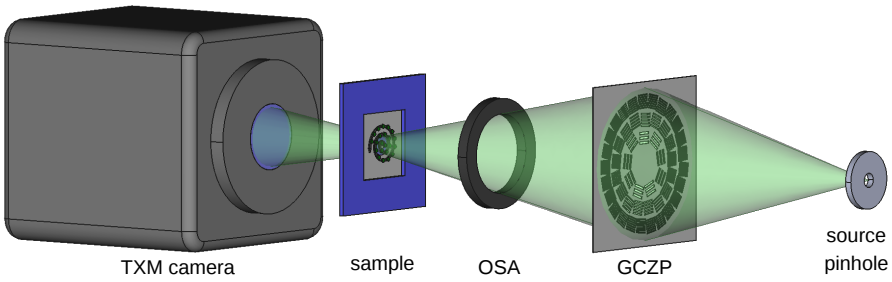

Fig. 2. A schematic diagram of the setup used for ptychographic imaging on the TwinMic beamline at Elettra. The source pinhole was 50μm in diameter and located about 2 m upstream of the GCZP, the TXM camera was located about 685 mm downstream of the sample plane. The GCZP had a 60 μm diameter central stop on its upstream side, and an order-selecting aperture (OSA) of 20 μm diameter was placed on the optical axis about 6 mm downstream of the GCZP to ensure that only the convergent first-order diffracted beams could reach the sample plane.The sample was a further 2 mm downstream of the OSA. The GCZP produced a focal spot ~ 6 μm diameter on the sample.

radial distance r from the pattern center was $r(\theta) = g\theta/2\pi$, normally with $g = 2\,\mu$m. Aperiodic patterns such as this help to avoid artifacts associated with rectangular raster scans [37], and can improve the quality of the ptychographic reconstructions [38]. Diffraction data were recorded at regular intervals of g along the path length, starting at the center of the spiral. To cover a square 24 μm × 24 μm scan field with 2 μm steps between scan positions, the spiral scan used 143 scan positions, while a conventional raster scan with the same step size would require 144 positions. The camera normally used for TXM imaging recorded far-field diffraction patterns for each point in the ptychography scan. This camera was a Princeton Instruments SX1300/TE back-face CCD detector located at a distance $L = 685$ mm downstream from the sample. The CCD is suitable for direct x-ray detection at energies up to ~ 800 eV, and a single readout cycle from the CCD produces 16-bit image data with a maximum of 1340 × 1300 pixels on a 20 μm pitch. The ptychographic datasets consisted of single scans of the sample field. Because of the limited dynamic range of the CCD detector it was operated in "accumulation" mode, which meant that there were a number of readout cycles from the detector at each scan position, with signal being accumulated after each readout. The number of readout cycles and the exposure time per cycle were constant throughout any one scan, so the overall exposure time was the same at each point in the scan. The exposure time per cycle was set to ensure that no CCD pixels would be saturated by the zero-order signal during the exposure time for that cycle. Thin, weakly absorbing samples would require quite short exposure times within each cycle, whereas longer exposure times were used for strongly absorbing samples. A small number of accumulation cycles could be used for strongly scattering samples where the diffraction signal could build up quite quickly, but weakly scattering samples would require a larger number of accumulation cycles to achieve reasonable statistics for the diffraction signal. Depending on the sample transparency, there were typically between 4 and 10 readout cycles at each scan position, with only a single CCD frame of accumulated data being recorded for each scan position. The overall exposure time per scan position is the product of the single-cycle exposure time and the number of accumulation cycles, and was typically in the range 3 s to 4 s. The data from each CCD frame were binned by a factor of 2 in each direction to give effective pixel areas of $\Delta^2 = 40\,\mu\text{m} \times 40\,\mu$m, and cropped to 512 × 512 pixels before reconstructions were carried out. The binning improved the signal-to-noise ratio of the diffraction data, reduced the readout time for each CCD frame, and reduced the array sizes

Optics EXPRESS

needed when computing the ptychographic reconstructions. The image resolution is determined by the angular extent of the diffraction data, and so it was not compromised by the binning operation.

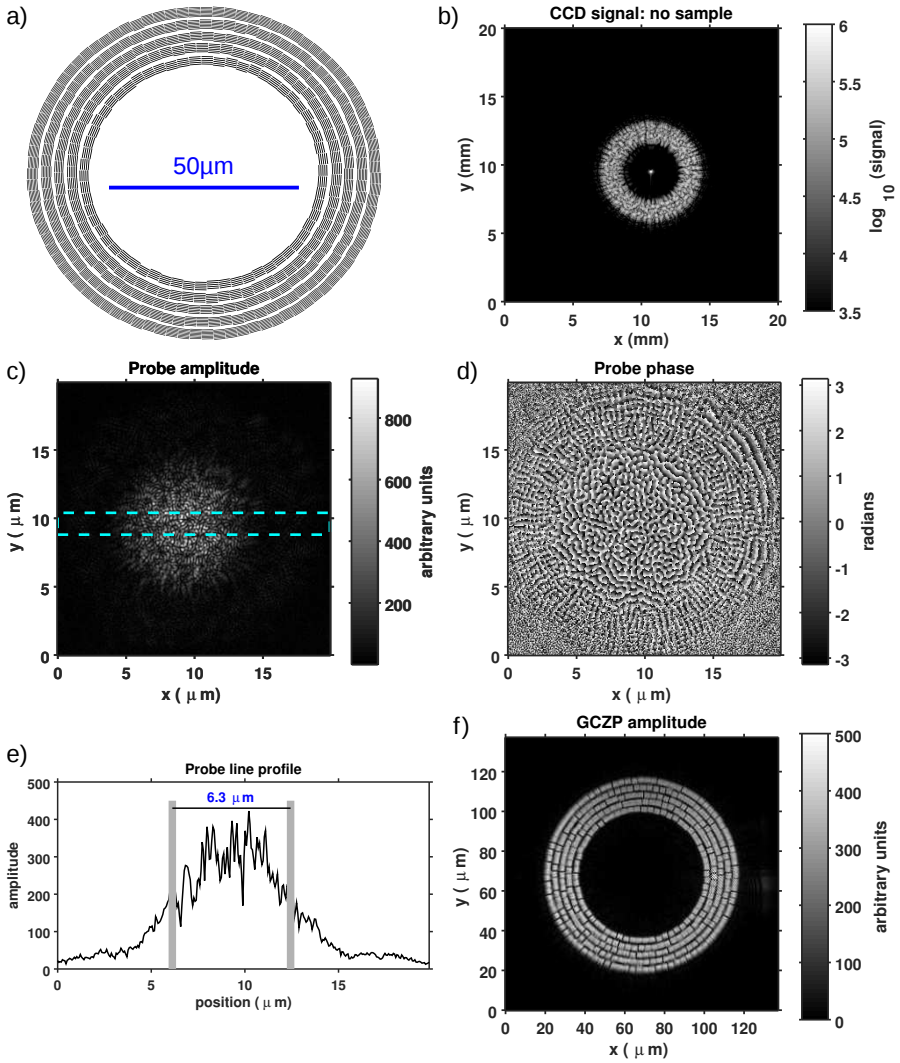

Fig. 3. a) A schematic showing the design of the randomized GCZP fabricated by Zone-plates.com. b) The signal distribution produced by the GCZP on the TwinMic CCD detector at a photon energy of 650 eV, in the absence of a sample. c) Ptychographic reconstruction of the probe amplitude distribution and (d) the probe phase distribution in the plane of the sample. e) A plot showing the average amplitude profile across the probe for the 25 rows of pixels within the dashed lines marked on (c). f) The amplitude distribution in the plane of the GCZP, obtained by back-propagating the complex probe upstream from the sample plane.

The optical setup used for ptychographic imaging with a randomized GCZP is shown schematically in Fig. 2. The design for a randomized GCZP suitable for use in ptychographic imaging on the TwinMic beamline is shown in Fig. 3(a). There are a total of 383 gratings located in 5 annular shells between an inner diameter of 60 μm and an outer diameter of 94 μm, with each grating occupying a 3 μm $\times$ 3 μm square field. The grating periods range from $\sim$ 520 nm for the

Optics EXPRESS

inner shell down to ~ 365 nm for the outer shell, and were chosen to give a focal length of 8 mm at a photon energy of 600 eV. The overall area of the gratings in this pattern is approximately half the area of a 94 μm diameter disc. Patterns based on this design were fabricated in 236 nm-thick tungsten film on a 100 nm-thick silicon nitride support film by Zoneplates Ltd [39]. A central stop of 60 μm diameter on the upstream side of the GCZP was used in combination with an OSA of 20 μm diameter that was placed on the optical axis about 6 mm downstream of the GCZP to ensure that only the convergent first-order diffracted beams from the GCZP could reach the sample plane. With binned CCD pixels of size $\Delta = 40\,\mu$m, the linear over-sampling ratio at a photon energy of 650 eV ($\lambda = 1.9$ nm), with a probe size $P = 6.3\,\mu$m, is given by $\lambda L/2P\Delta = 2.6$. An over-sampling ratio ≥ 1 is usually considered sufficient for successful ptychographic reconstructions, but this constraint can be relaxed in some circumstances [17].

3. Results

Figure 3(b) shows the signal distribution produced on the CCD in the absence of a sample. If a pinhole aperture of diameter P had been used instead to define the probe, the central lobe of the Airy diffraction pattern from the aperture would have illuminated an area of diameter $\sim 2.44\lambda L/P$ on the CCD, where L is the distance to the detector and λ is the illumination wavelength, whereas both the GCZP and the FZP described above will spread the diverging cone of illumination downstream from the focal plane over an annulus on the detector with outer diameter $\lambda L/d_N$. The ratio of the annulus area to that of the central lobe of the Airy pattern is $(P/2.44d_N)^2/2 \approx 68$ when $P = 5\,\mu$m and $d_N = 176$ nm, so the use of a focusing element to form the probe will spread the undiffracted light emerging from the sample plane over a detector area almost 70× larger than that illuminated when a simple probe-defining aperture is used, an important consideration when using detectors such as CCDs.

Ptychography scans of the Siemens-star test pattern shown in Fig. 4(a) allowed a reconstruction of the probe wavefront incident on the sample using the ePIE algorithm [5] with the object update parameter set to $\alpha = 0.5$. Initial ptychographic reconstructions of the test pattern started with a uniform circular disc as the probe guess, and this led to reasonable first estimates of the probe and sample. Subsequent reconstructions of the test pattern then used the first estimates of probe and sample as the starting conditions: for the first few tens of iterations only the probe was updated, and thereafter both the probe and sample estimates were updated to get the final reconstructions of the complex probe and sample transmittance.The amplitude of this wave is shown in Fig. 3(c), while Fig. 3(d) shows the corresponding phase reconstruction (without phase unwrapping), from which we can infer that the randomized GCZP has successfully produced a high level of phase diversity. The pixel size in the probe reconstructions can be calculated as $\lambda L/N_D\Delta \approx 65$ nm, where $N_D = 512$ is the number of (binned) pixels along one edge of the square CCD frames used in the reconstructions. The localised intensity variations within the the central lobe of the probe amplitude resemble a speckle pattern, and mean that it is difficult to estimate the probe size from a single line profile. Figure 3(e) plots a line profile formed by averaging over 25 rows of the image that lay between the two dashed lines in Fig. 3(c). This profile shows that the GCZP produced a focal spot of diameter 6.3 μm on the sample, as measured by the full-width at half-maximum (FWHM) value. For comparison, a conventional FZP with an outer diameter of 94 μm and the same focal length as the GCZP should have an outer zone width $d_N \sim 176$ nm, and this would produce a diffraction-limited probe size $\sim 1.22d_N \approx 215$ nm in its focal plane. Figure 3(f) shows the calculated wave amplitude after propagating the complex probe back upstream to the plane of the GCZP. The Fresnel algorithm [40] was used to propagate the retrieved wave upstream, as this algorithm is suitable when dealing with beams that converge or diverge between the two planes. There is a reassuringly strong resemblance between the design shown in Fig. 3(a) and the reconstructed pattern in Fig. 3(f). However, as the upstream propagation involves a beam that diverges towards the GCZP plane, the effective pixel size of this reconstruction is calculated

Optics EXPRESS

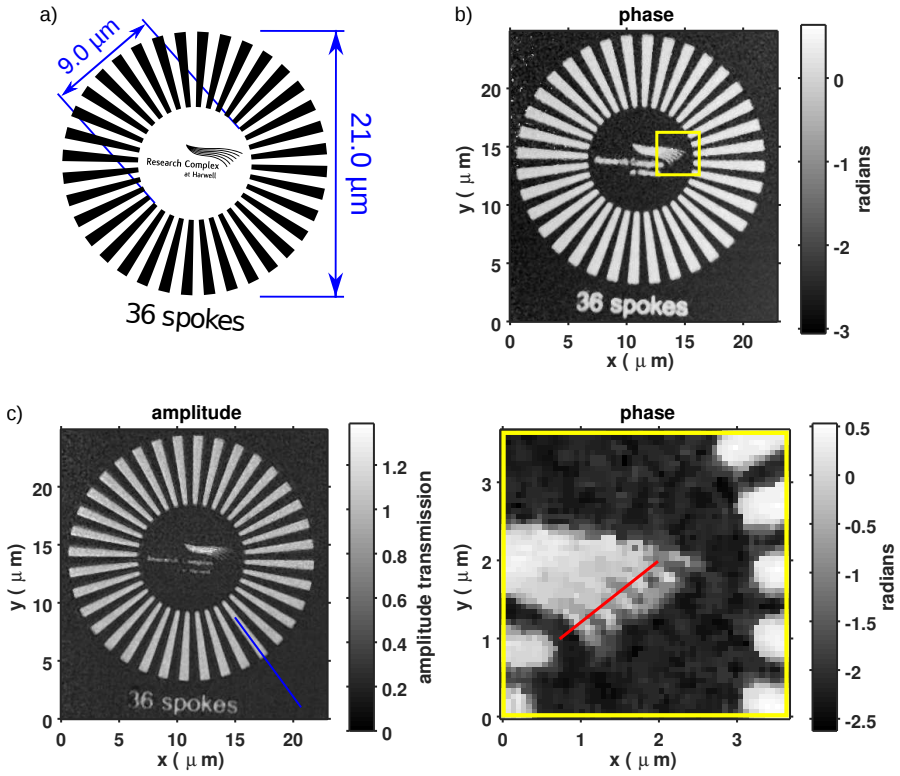

Fig. 4. a) A schematic of the test pattern design that was etched into a 150 nm-thick tungsten film on a 100 nm-thick silicon nitride support film. Ptychographic reconstructions show b) the phase and c) the amplitude of the sample transmittance for the test pattern at an x-ray energy of ~ 650 eV, with the blue line on (c) marking where line profiles were taken along an open spoke. The overall exposure time for each position in the ptychography scan was 3 s. d) A close-up view of the region highlighted by the yellow square in (b), with the red line marking where line profiles have been taken from the amplitude and phase reconstructions.

to be 523 nm, which is larger than the largest grating period present in the GCZP, so it is not possible to resolve individual grating features. It is also unclear whether the orientation of the reconstruction is the same as the design shown in (a), since this depends on how the GCZP was mounted in the TwinMic chamber.

Scans of the test pattern in Fig. 4(a) were carried out at 650 eV over a 24 μm × 24 μm scan field with a scan step of 1.5 μm and an overall exposure time of 3 s at each scan position. The linear over-sampling ratio was 2.6, and the pixel size in the image reconstructions was again 65 nm. Figures 4(b) and 4(c) show the phase and amplitude reconstructions of the Siemens-star test pattern shown in Fig. 4(a). The pattern was etched into 150 nm-thick tungsten film on a 100 nm-thick silicon nitride support film. The blue line on Fig. 4(c) shows where line profiles were taken radially inwards along an open spoke in the amplitude and phase reconstructions, and these profiles are plotted in Fig. 5(a) and (b).

Table 1 shows a comparison between the measured amplitude and phase transmission values in Fig. 4(e) and the values expected at 650 eV using the semi-empirical values for x-ray optical constants tabulated by Henke *et al.* [41]. The values in the open spoke areas are consistent with free space, suggesting that the silicon nitride support film has been completely removed from these extended open areas during fabrication of the pattern. This is often found to occur when

Optics EXPRESS

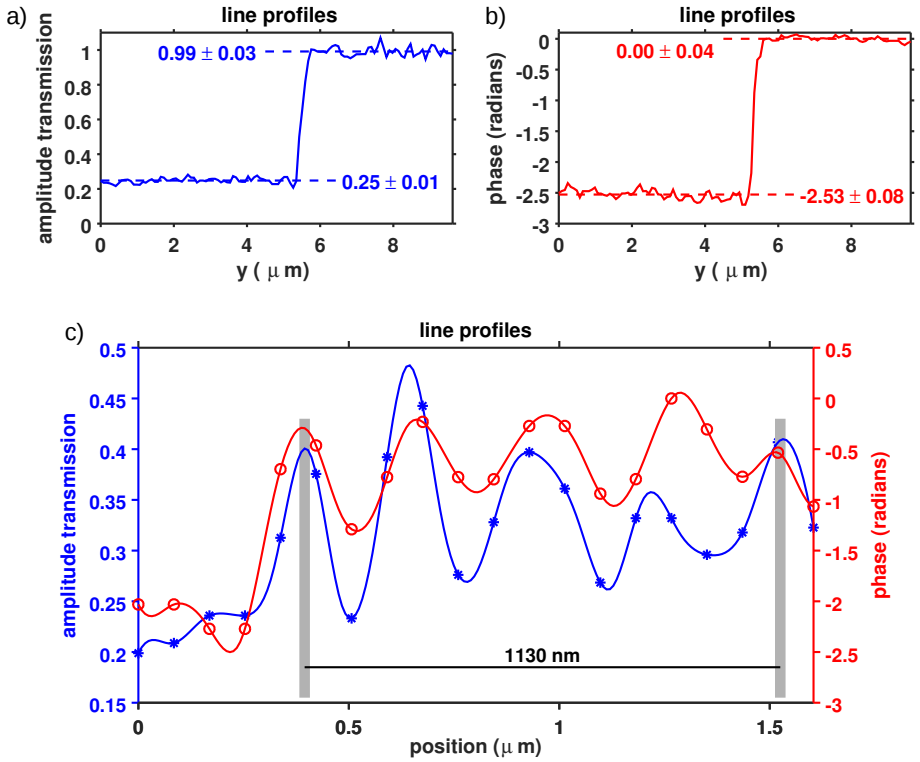

Fig. 5. Line profiles showing a) the amplitude transmission and (b) the phase taken radially inwards along the blue line shown in Fig. 4(c). The dashed lines show the mean values of the signal in the high and low regions of these profiles. c) A plot showing the amplitude (blue stars) and phase signals (red circles) sampled along the red line shown in Fig. 4(d). The solid lines are quartic spline curves fitted to the sampled data, and are intended only as a guide to the eye.

the same test pattern includes both high-resolution features and quite coarse structures etched into relatively thick tungsten films, since the etching conditions needed to achieve good aspect ratios for the high-resolution features are sufficient to remove exposed silicon nitride support membrane from the coarse structures [42]. The mean transmission values in the absorbing film outside the spoke are in good quantitiative agreement with those expected for 150 nm of tungsten on top of 100 nm of silicon nitride.

Table 1. A comparison of measured and expected transmission values at 650 eV for the test pattern shown in Fig. 4. Expected values are based on tabulated values of soft x-ray optical constants [41].

	Amplitude		Phase (radians)	
	Measured	Expected	Measured	Expected
Open spoke	0.99 ± 0.03	1	0.00 ± 0.04	0
150 nm tungsten + 100 nm silicon nitride	0.25 ± 0.01	0.26	−2.53 ± 0.08	-2.56

A magnified view of the banner that forms part of the “Research Complex at Harwell” logo is shown in Fig. 4(d), and the red line on this figure indicates where line profiles were taken across

Optics EXPRESS

the fronds of this banner to get an estimate of the spatial resolution achieved in the ptychographic reconstructions. The signal profiles are plotted in Fig. 4(f): the solid lines are obtained by a quartic spline fit to the marked points and are intended only as a guide to the eye. These profiles straddle 4 periods of the frond pattern, and show that a period of ~ 280 nm can be resolved in both the amplitude and phase reconstructions, corresponding to feature sizes (half-period resolution) ~ 140 nm. If the diffraction data were restricted to the angular extent of the brightfield cone landing on the detector, the reconstructed images should be able to resolve spatial periods of order $\lambda/\theta_c \sim 350$ nm, where θ_c is the half-angle of the brightfield cone produced by the GCZP, so the measured resolution suggests that the useful diffraction data extends some way outside the brightfield cone shown in Fig. 4(b), but does not extend to the edge of the CCD detector. The resolution reported here is broadly similar to that previously reported by other CDI measurements on the TwinMic beamline [30, 43].

A careful inspection of the phase image in Fig. 4(b) shows that, for sample features where there are relatively large open areas, such as the radial spokes, the sharp boundaries of the tungsten film appear to be displaced slightly towards the tungsten film, when compared with the corresponding edge positions for the amplitude image in Fig. 4(c). The open spokes thus appear slightly wider than their amplitude counterparts, but it is not clear that this is due to a difference in resolution: if the edge profiles in Fig. 5(a) and (b) are overlayed, the edge sharpness is seen to be the same for both amplitude and phase. The edge shifts themselves are quite small, typically corresponding to about 1 pixel of the reconstructed images (~ 65 nm) for the test pattern images) and so are well below the estimated image resolution.

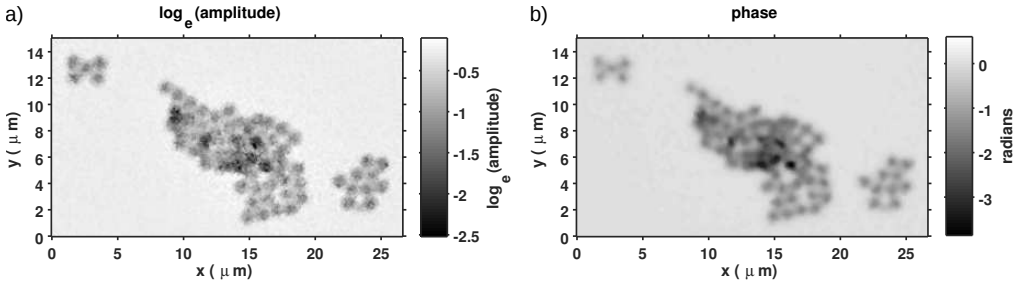

Fig. 6. Ptychographic reconstructions at a photon energy of ~ 500 eV of a) the logarithmically-scaled amplitude and b) the phase of the transmission function for an assembly of polystyrene spheres that are 1.09 μm in diameter, supported on a thin holey carbon film. The exposure time for each position in the ptychography scan was 4 s.

Figures 6(a) and 6(b) show further examples of successful amplitude and phase reconstructions, this time from a more weakly absorbing object that is perhaps more typical of the samples often studied by soft x-ray microscopy. The setup used for the polystyrene spheres was the same as for the test pattern, except that the incident photon energy was reduced to ~ 500 eV, requiring a proportional reduction in the distance from the GCZP to the sample. The overall exposure time at each scan position was 4 s, the scan field was 24 μm × 24 μm with a scan step of 2 μm. The probe size at the GCZP focus is independent of the energy and was again 6.3 μm, while the linear over-sampling ratio increased to 3.4. In this case, the initial estimate of the complex probe was based on that found from the reconstructions of the test pattern. These images show small assemblies of 1.09 μm-diameter polystyrene spheres supported on a thin holey carbon film, with the individual spheres clearly resolved, as the sphere diameters are about 7× larger than the half-period resolution estimate. There is no significant difference in resolution between the two images; the most obvious difference between them is that the amplitude image is noisier than the phase image, and this is related to the complex refractive index $n = 1 - \delta - i\beta$ for polystyrene. The ratio $\delta/\beta = 3.6$ at 500 eV (assuming a typical composition $(C_8H_8)_n$ for polystyrene), so

Optics EXPRESS

the phase signal should be stronger than the amplitude signal. The spatial resolution in these reconstructions should also be similar to that found for the test pattern in Fig. 4 although the polystyrene spheres may not scatter as strongly as the tungsten test pattern, so the angular extent of measurable diffraction data may be smaller.

Clearly, to achieve higher resolution reconstructions from either the tungsten or polystyrene samples it is necesary to increase the angular extent of the diffracted light that contributes to the reconstructions. For example, the use of longer signal dwell times may have allowed weak signals closer to the edge of the detector to contribute to the reconstructions. Moving the CCD closer to the sample plane would concentrate the scattered beams on to fewer detector pixels and this could help to raise some weaker signals above the detector noise level, but mechanical constraints of the TwinMic microscope meant it was not practicable to move the CCD detector any further upstream.

4. Discussion

It is worth noting that the regular GCZPs first produced for use in a TXM [32] were significantly larger than the ones reported here: the individual gratings were approximately 50 μm × 50 μm square within polygonal shells that lay between an inner diameter of 500 μm and an outer diameter of 1 mm. Our much smaller randomized GCZP patterns fit comfortably into a single drawing field for an electron beam lithography system, and the minimum feature sizes ~ 180 nm are readily produced.

The relatively small outer diameter of the GCZP pattern ensured that it could be illuminated coherently on the TwinMic beamline without sacrificing too much flux, and that it was comparable to the size of the random pinhole arrays used as x-ray diffusers for previous ptychography measurements [30]. However, the GCZP allows a much larger fraction of the light illuminating it to contribute to the x-ray probe. Consider, for example, a GCZP of diameter D with a central stop occluding a disc of diameter γD, where $\gamma < 1$. Ignoring the small opaque spaces between active polygonal shells, a fraction $\left(1-\gamma^2\right)\eta_1$ of the light incident on the GCZP can contribute to the probe signal, where η_1 is the first-order diffraction efficiency of the individual gratings. On the other hand, a probe-defining aperture of diameter P collects only a fraction $(P/D)^2$ of the light falling on a random pinhole array of diameter D. Choosing $P = 5$ μm, $D = 100$ μm, and $\eta_1 = 0.1$ shows that the GCZP will illuminate the sample with about 30× more signal than the combination of a diffuser and a pinhole aperture.

A conventional Fresnel zone plate with the same outer diameter D, the same central stop diameter γD, and the same diffraction efficiency, would direct the same fraction of the incident light into the first-order focus as the GCZP, so the two forms of zone plate will have similar benefits in terms of the overall signal throughput. Both the GCZP and the FZP will spread the diverging cone of illumination downstream from the focal plane over a similar area of the detector, so they will produce the same beneficial reduction in the dynamic range of the detected signal. However, the FZP produces a diffraction-limited probe size ~ $1.22d_N \approx 215$ nm in its focal plane that is much smaller than the ~ 6.3 μm probe produced by the GCZP, so the required step size in ptychography scans would be proportionately smaller, resulting in longer scan durations if the exposure times at each scan position are kept the same. In principle, the exposure time could be reduced in direct proportion to the reduction in the area of the probe, so that the overall x-ray exposure of the sample is the same for either the large or small probe, but there are a number of practical difficulties with this approach. For example, the probe sizes discussed above imply that the exposure time for the smaller probe should be reduced by a factor of $(6300/215)^2 \approx 860$, resulting in exposure times that are very much smaller than the readout time of the CCD, and may even be smaller than the CCD controller is capable of providing. In addition, the total signal in each CCD frame will be reduced, and the number of frames to be processed will be increased, by the same factor, resulting in a very large volume of much noisier data. A recent analysis by

Optics EXPRESS

Jacobsen *et al.* [44] has introduced a useful parameter known as the "ptychographic resolution gain", G_p, which is a ratio defined as the probe diameter divided by the reconstructed image pixel size. In the notation used in the present paper, $G_p = PN_D\Delta/\lambda L$. Ptychography with a conventional FZP at focus corresponds to a small value of G_p, whereas ptychography using a GCZP corresponds to a large value of G_p. For the conditions used to acquire the test pattern data in Fig. 4, $G_p \approx 100$. Under certain conditions, optimised setups with either large or small values of G_p can be shown to produce the same volume of diffraction data for the ptychographic reconstructions. There are some advantages in using a setup with a small G_p, but a setup with a large G_p is desirable when thermal noise and readout noise are present in detectors such as CCDs, and where significant time overheads are associated with the collection of the diffraction data, as is the case with the setup we have described on the TwinMic beamline.

Apart from its large G_p value, the other desirable features of the GCZP probe are its enhanced phase diversity arising from the contributions of a large number of random elements, and the local speckle-like variations of the probe amplitude that will broaden the spatial frequency spectrum of the probe. The FZP probe size can be increased by defocusing the FZP to produce a setup with large G_p: in this case a defocus of $\sim 540\,\mu$m would produce a spot with $\sim 6.3\,\mu$m diameter at 600 eV. The intensity distribution in the defocused FZP probe will be less uniform than at focus, giving a desirable increase in the spatial frequency spectrum of the probe, but it will lack the randomized phase produced by the randomized GCZP. One advantage that does remain with the FZP is that it can always be switched back into a setup with a small G_p, or even be used in a conventional scanning x-ray microscope. However, a high resolution FZP is considerably more challenging to fabricate, and is likely to be much more expensive as a result.

The FZP could also be used in conjunction with a random diffuser to increase the phase diversity, but at soft x-ray energies this additional element in the beam path will reduce the overall signal throughput, since there will be significant absorption of the beam by the diffuser. For example, at 600 eV, a diffuser consisting of random holes etched into a silicon nitride membrane will have an optimum thickness of ~ 540 nm with a hole area density $\sim 30\%$, and such a diffuser absorbs $\sim 56\%$ of the incident intensity. For soft x-ray applications in particular, it is thus more efficient to use a single randomized GCZP to achieve the desired combination of benefits rather than to use a separate FZP and a diffuser. This philosophy was also manifest in the design of other forms of diffractive optical elements for x-ray applications [45–48].

In this paper we have not made an explicit comparison between the quality of ptychographic reconstructions achieved with different levels of phase diversity in the probe illumination, as the benefits of enhanced phase diversity have already been explored in other publications, both theoretically [12, 13, 15] and experimentally [10, 11, 28–31]. A recent analysis of alternating projection (AP) algorithms [49] used in ptychography includes numerical simulations that compare the performance of ptychographic probes produced by a small circular lens incorporating an axial beamstop (analgous to the use of FZPs in x-ray microscopy) with the performance of a band-limited random (BLR) lens. The BLR lens consists of an annular aperture within which the phase of the illumination takes random values, and where the amplitude is adjusted iteratively to produce a circular focus spot. Their analysis shows that the use of the BLR lens, in conjunction with the use of "phase synchronisation" methods to generate initial guesses that are fed into the reconstruction algorithms, can lead to significant improvements in the convergence of both AP and relaxed averaged alternating reflection algorithms [50]. While we have not repeated the analysis for the case of a randomized GCZP, Figs. 3(b), (c) and (d) show there are strong similarities between the probe produced by the GCZP design reported in this paper and the probe produced by the BLR lens described in [49], so we believe that similar benefits could well be associated with the use of a randomized GCZP in ptychography.

Optics EXPRESS

5. Conclusions

The results in this paper show that randomized GCZPs can be used successfully to produce μm-scale probes for soft x-ray ptychography, and to deal with some widely-recognised practical difficulties when collecting ptychographic data. The GCZP produces a probe with a high ptychographic resolution gain G_p and this form of optical element is well suited to soft x-ray ptychography measurements that rely on charge-integrating 2D detectors such as CCDs. The GCZP provides a significant increase in signal throughput compared to the use of a probe-defining aperture (whether or not this is combined with a separate phase-randomizing component), it spreads the light that is undiffracted by the sample over an extended detector area, and provides control over the phase diversity, since the number of gratings in the GCZP pattern determines the range of phases present in the probe. The randomized GCZP design is relatively straightforward to fabricate, so it offers an attractive and cost-effective option as a probe-forming optical element for ptychography measurements on the TwinMic beamline at Elettra and elsewhere.

Funding

U.K. EPSRC grant EP/I022562/1; U.K. BBSRC grant BB/H022597/1; U.S. Department of Energy, Office of Basic Energy Sciences grant DE-SC00112704.

Acknowledgments

We are grateful to George Kourousias and Roberto Borghes of the IT group at Elettra for their support prior to and during the beamtime on TwinMic. P. S. Charalambous of Zoneplates Ltd manufactured both the randomized grating condenser zone plate and the tungsten test pattern to our design.